AD-A148 071 BEAM PROPAGATION STUDY: STABILIZATION OF THE RESISTIVE HOSE INSTABILITY I.. (U) MISSION RESEARCH CORP ALBUQUERQUE NM R J ADLER ET AL. AUG 84 AMRC-R-598 1/1

UNCLASSIFIED AFOSR-TR-84-0923 F49620-83-C-0128 F/G 20/8 NL

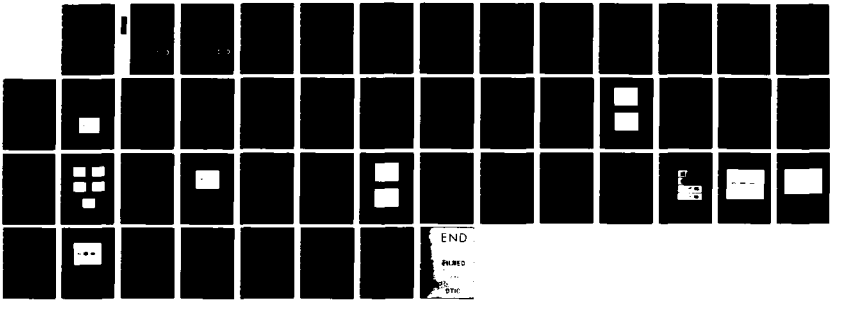

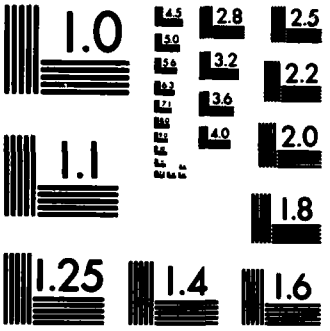

AFOSR-TR- 84-0923

(5)

AMRC-R-598
Copy 6

FINAL REPORT

BEAM PROPAGATION STUDY: STABILIZATION OF THE RESISTIVE HOSE INSTABILITY IN INTENSE ELECTRON BEAMS

R. J. Adler
G. F. Kiuttu
R. J. Richter-Sand

August 1984

Prepared for: Air Force Office of Scientific Research
Physics Directorate
Bolling Air Force Base
Washington, DC 20332

and

Air Force Weapons Laboratory
Applied Physics Division
Kirtland Air Force Base
New Mexico 87117

Under Contract: F49620-83-C-0128

and

F29601-83-C-0050

Prepared by: MISSION RESEARCH CORPORATION
1720 Randolph Road, S.E.
Albuquerque, New Mexico 87106

AMRC-R-598
Copy ____

FINAL REPORT

BEAM PROPAGATION STUDY: STABILIZATION OF THE RESISTIVE HOSE INSTABILITY IN INTENSE ELECTRON BEAMS

August 1984

R. J. Adler
G. F. Kiuttu
R. J. Richter-Sand

Prepared for: Air Force Office of Scientific Research
Physics Directorate
Bolling Air Force Base
Washington, DC 20332

and

Air Force Weapons Laboratory
Applied Physics Division
Kirtland Air Force Base
New Mexico 87117

Under Contracts: F49620-83-C-0128

and

F29601-83-C-0050

Prepared by: MISSION RESEARCH CORPORATION
1720 Randolph Road, S. E.
Albuquerque, New Mexico 87106

UNCLASSIFIED

SECURITY CLASSIFICATION OF THIS PAGE (When Data Entered)

REPORT DOCUMENTATION PAGE	READ INSTRUCTIONS BEFORE COMPLETING FORM
1. REPORT NUMBER **AFOSR-TR- 84-0923** 2. GOVT ACCESSION NO. AD-A148 071	3. RECIPIENT'S CATALOG NUMBER
4. TITLE (and Subtitle) BEAM PROPAGATION STUDY: STABILIZATION OF THE RESISTIVE HOSE INSTABILITY IN INTENSE ELECTRON BEAMS	5. TYPE OF REPORT & PERIOD COVERED 1 JUL 83 - 30 APR 84 FINAL
	6. PERFORMING ORG. REPORT NUMBER AMRC-R-598
7. AUTHOR(s) R. J. Adler G. F. Kiuttu R. J. Richter-Sand	8. CONTRACT OR GRANT NUMBER(s) F49620-83-C-0128
9. PERFORMING ORGANIZATION NAME AND ADDRESS MISSION RESEARCH CORPORATION 1720 Randolph Road, S.E. Albuquerque, New Mexico 87106	10. PROGRAM ELEMENT, PROJECT, TASK AREA & WORK UNIT NUMBERS 61102F 2301/A7
11. CONTROLLING OFFICE NAME AND ADDRESS Air Force Office of Scientific Research Physics Directorate Bolling Air Force Base, DC 20332	12. REPORT DATE August 1984
	13. NUMBER OF PAGES 44
14. MONITORING AGENCY NAME & ADDRESS(if different from Controlling Office)	15. SECURITY CLASS. (of this report) UNCLASSIFIED
	15a. DECLASSIFICATION DOWNGRADING SCHEDULE

16. DISTRIBUTION STATEMENT (of this Report)

Approved for public release; distribution unlimited.

17. DISTRIBUTION STATEMENT (of the abstract entered in Block 20, if different from Report)

18. SUPPLEMENTARY NOTES

19. KEY WORDS (Continue on reverse side if necessary and identify by block number)

Electron Beam
Beam Propagation
Resistive Hose Instability
Rotating Beams
E-Layers
Air Conductivity
B-Field Alignment

20. ABSTRACT (Continue on reverse side if necessary and identify by block number)

A series of experiments has been performed to investigate the effect of unidirectional beam particle rotation on the resistive hose instability. Using the 4 MV, 100 kA, IBEX accelerator in a foil diode configuration, hose growth for hollow, partially hollow, and non-rotating Bennett profile beams was investigated. We found that partially hollow, rotating beams were most stable. In particular, they were more stable than non-rotating Bennett profile beams both in terms of the growth rate in ~~cm^{-1}~~ per cm and in the growth per betatron wavelength. (cont'd)

DD FORM 1 JAN 73 1473 EDITION OF 1 NOV 65 IS OBSOLETE

UNCLASSIFIED

SECURITY CLASSIFICATION OF THIS PAGE (When Data Entered)

The observed reduction in instability growth rate per betatron wavelength over Bennett profile beams was a factor of 2.5. Stable propagation for >6 betatron wavelength (the full experiment length) was observed in some shots where the beam was well aligned. Broadened return current profiles and long plasma decay times were also observed, consistent with our present understanding of high current mode propagation.

TABLE OF CONTENTS

LIST OF ILLUSTRATIONS

LIST OF ILLUSTRATIONS (continued)

EXECUTIVE SUMMARY

Directed energy weapons have the potential to revolutionize modern warfare and greatly affect national defense policies. The application of high-energy particle beams as directed energy weapons is particularly promising because of their ability to penetrate targets. The realization of this concept is dependent on the solution of major technical issues in the areas of pulsed power, particle accelerators and beam-target interactions.[1] These technical problems can probably be overcome with the expenditure of sufficient technical effort.

The physics of beam propagation may, however, prevent delivery of sufficient energy over the distances required to make beams practical as weapons. Endoatmospheric propagation remains a key issue that may not yield to a massive research effort. Basic physics questions about the growth rates and nature of instabilities encountered during beam pulse transmission through the atmosphere remain unresolved. The complexity of beam propagation physics and air chemistry makes the prediction of beam behavior difficult. Clearly, the issue of propagation will not be fully resolved until full-scale experiments with accelerators having weapons-grade parameters are performed. It is also clear that one cannot wait for the advent of such experiments, because beam propagation will have a significant role in determining the optimal weapon accelerator parameters.

The most important issue in intense electron beam propagation in the atmosphere is the resistive hose instability. This effect, which results from the resistive diffusion of plasma magnetic fields, has previously been studied by a number of authors.[2-5] Only two techniques are known to suppress the instability - reduction of the plasma resistivity by lowering the pressure (not practical in the atmosphere) and increasing the emittance by foil scattering. Simply increasing the emittance in order to stabilize the instability results in an energy density on target which is thought to be too small to be useful.

In previous experiments,[6,7] a third technique for reducing hose growth was observed - the introduction of net rotation into the electron distribution. These results were tentative, and skeptics argued that, while the hose stable propagation distance increased, the increase in beam radius due to rotation was larger yet.

In order to resolve this question we have performed a series of experiments using the (4 MeV, 100 kA) IBEX accelerator. The goal of the experiment was to compare the instability growth of beams with and without rotation, while keeping all other parameters fixed. Various rotating beam profiles were investigated by using different types of cathodes (non-rotating profiles usually tend towards a Bennett profile), and only one drift tube pressure - 630 Torr was used.

A prerequisite of the hose study was the characterization of the beam properties in equilibrium. Time resolved Faraday cup measurements and blue cellophane time integrated measurements were used to measure the beam radius. Position monitors were used to characterize the magnetic centroid offset of the beam at injection. Characterization measurements are presented in Section 2. Those diagnostics used in the experiment which have not yet been described elsewhere are discussed in Section 1.

The most important experimental results are given in Section 3, the rotating hose growth measurements. We find that rotating beams are, in general, more stable than nonrotating beams when some small beam current is present on axis. Various P_θ distribution functions were produced by using different types of cathodes, and one distribution was found to be superior. The so called 'bullet' tip produced a beam which was primarily annular in shape, with an approximately uniform, lower current beam running down the center of the annulus. This type of beam was found to be most stable. This result is important both as a technique for improving propagation in future experiments and in increasing our understanding of the resistive hose instability.

Discussion of the mechanisms for rotational hose stabilization is presented in Section 5. The most probable cause of rotational hose stabilization is the increased shear in betatron wavelength due to rotation. This stabilizing mechanism is discussed along with several others in Section 5.

SECTION 1

DIAGNOSTICS AND EQUIPMENT

A number of the diagnostics used in this experiment were described in a previous report.[5] The most important measurement was that of the transverse position of the magnetic centroid, discussed in detail in Section 1.1. Magnetic field alignment is reviewed in Section 1.2. Other miscellaneous equipment is described in 1.3.

1.1 MAGNETIC CENTROID MEASUREMENT TECHNIQUES

Two types of magnetic probe arrays were used in the experiment. The first was developed under a previous contract with AFOSR and is described in detail elsewhere.[5] The second type of probe is shown schematically in Fig. 1.

The measured voltage in any loop is related to the transverse position δ by

$$\delta = R - \frac{\mu_o I A}{2\pi\tau V}$$

where R and A are defined in Fig. 1. I is the beam current, V is the measured,integrated voltage, and τ is the integrator time constant. In practice, if one has identical detectors spaced azimuthally 180° apart, then one may subtract the common signal R and a direct measure of δ results. In practice, errors in the area A and in the exact specification of the summing boxes must be compensated. We have found that commercial subtracting boxes are often not sufficiently accurate to allow use of this technique with the required accuracy.

In the magnetic probe array shown in Fig. 1, the loop area can be adjusted by rotating the UT-250 rigid coax. The protruding center coax conductor is not straight, rather, it has a slight bend, so that when the

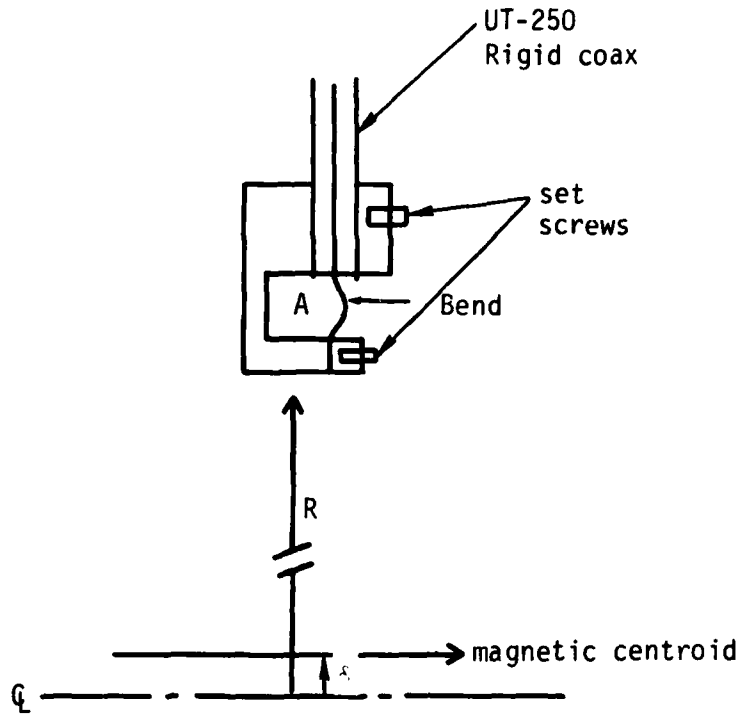

Figure 1. Adjustable magnetic loop schematic.

orientation of the wire is changed, the area of the loop is increased or reduced. The probe/subtractor pairs were placed on a calibration stand and adjusted until, for an on-axis current, no signal was measured. Individual loop areas were then calibrated to obtain an absolute calibration value. Displacements could easily be measured to less than 1 mm (1%) after this procedure was followed. For measurements near the anode, where large external magnetic fields were present, inductive shunts were used to short the high amplitude low frequency background signals.

1.2 MAGNETIC FIELD ALIGNMENT

One crucial aspect of this experiment was alignment of the magnetic axis with respect to the geometric axis defined by the extraction foil and drift tube. Low energy electron gun systems for alignment were not useful on the IBEX accelerator because ambient transverse fields in the region of the cathode were found to be of the order of several gauss.

The AMFAD (Accelerator Magnetic Field Anomally Detector) invented by Carl Ekdahl, consists of nothing more than a multiple turn coil mounted at an angle θ on a rapidly rotating shaft, as shown in Fig. 2. From Faraday's Law the induced voltage is given by:

$$V = \frac{\partial}{\partial t} \left(- N \vec{A} \cdot \vec{B} \right) \tag{1}$$

where

$$\vec{A} \cdot \vec{B} = [A B \cos\theta \cos\phi + A B \sin\phi \sin\theta \sin\omega t], \tag{2}$$

the area A is given by: $A = \pi a^2 / \cos\theta$, ω is the angular frequency of rotation and ϕ is the relative angle of the magnetic field to the geometric axis.

The algebra yields a sensitivity in <u>millivolts</u> of:

$$V_{p-p} = 6.58 \times 10^{-6} \; N \text{ (turns)} \; f\text{(rpm)} \; a^2 \; (\text{cm}^2) \times B(\text{G}) \sin\phi \tan\theta \tag{3}$$

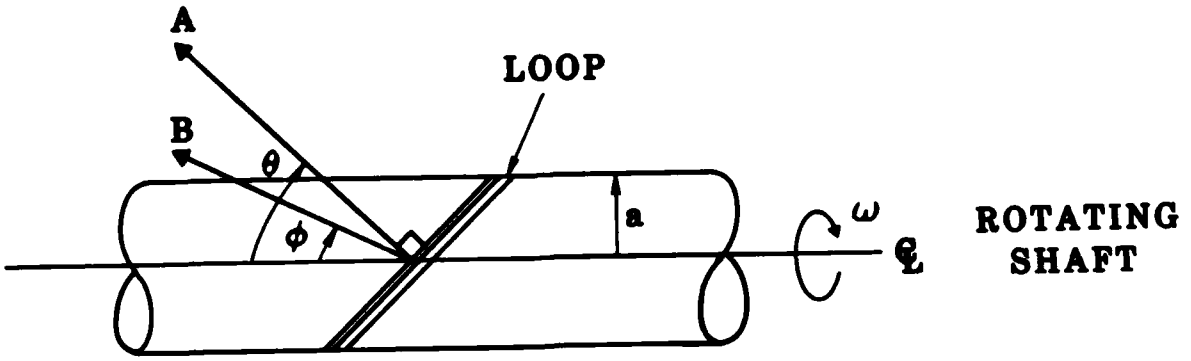

Figure 2. AMFAD diagram.

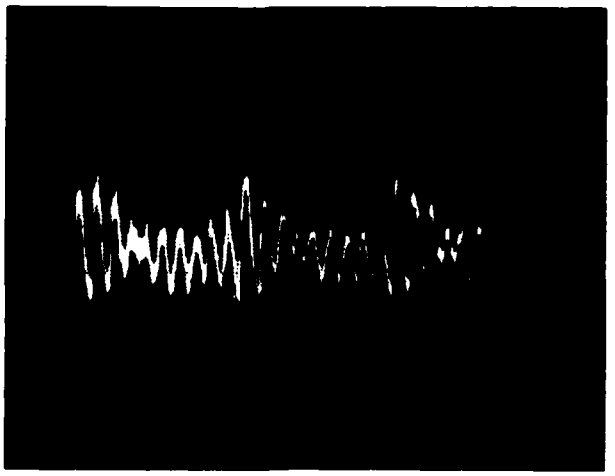

Figure 3. AMFAD output voltage waveform.

Even selecting a reasonable number of turns and a rapidly rotating coil, the signal is very small. MRC personnel modified the basic design to include an op amp and noise filtering circuits which provided sufficient gain to permit alignment measurements.

A variation of the basic technique was incorporated into the AMFAD alignment procedure. A time varying magnetic field was produced by connecting the field coil to a pair of filament transformers wired in series (12.6 volts, 60 Hz). The static AMFAD signal with the high pass noise filter removed was noted with the field on. The AMFAD drive motor was then engaged and the signal was observed on a Tektronics 475 oscilloscope as shown in Fig. 3. The 500 Hz motor frequency is superimposed on the 60 Hz envelope of the detected B-field. Alignment was performed by minimizing the observed peak-to-peak signal through manipulation of the magnet orientation.

The remaining misalignment ϕ can then calculated in the following manner:

$$\phi \approx B_r/B_z = \frac{V_{500}}{V_{60}} \times \frac{\omega_{60}}{\omega_{500}} \qquad (4)$$

Magnet alignment using this procedure removed the complication of the transverse perturbing fields in the region of the IBEX beamline.

1.3 MISCELLANEOUS EQUIPMENT

The IBEX accelerator is a so called 'Isolated Blumlein' device topologically similar to the Radial Isolated Blumlein described in the literature.[8] Because of the unique design of these devices, fast voltage rise times with zero prepulse are obtained. The electron energy was derived from the machine resistive voltage monitor, since the 'flat top' of the voltage pulse is sufficiently long on many shots to justify taking the peak voltage as the peak-electron energy without inductive correction. Typical voltage and current waveforms are shown in Fig. 4.

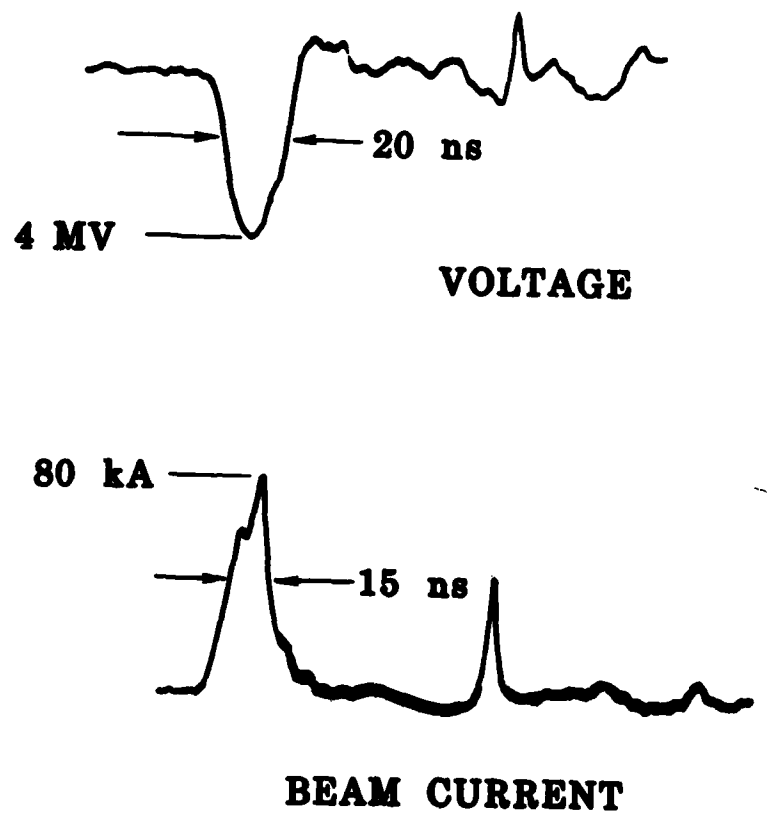

Figure 4. Typical IBEX voltage and current waveforms.

Beam current density was observed with a Faraday cup array consisting of 8, UT-141 coaxial cables mounted in a carbon block. All detectors were spaced 2 cm apart starting at r = ± 1 cm. The four center detectors had brass inserts which attenuated signals by a factor of ~ 8 to avoid cable breakdown.

SECTION 2

EXPERIMENTAL DESCRIPTION AND BEAM EQUILIBRIUM RESULTS

A schematic of the experimental setup is shown in Fig. 5. The beam energy is fed out of the IBEX accelerator vacuum diode and through the pumping manifold on a 1.27 cm diameter cathode shank. Various cathode tips are fastened to this shank, while the anode-cathode gap was kept at a fixed value of 3.1 cm. Foils of 125 μm thick titanium provided the air/vacuum interface, resulting in an RMS beam scattering angle of 10°.

A large dipole magnetic field coil encircled the cathode shank and imposed a rapidly diverging magnetic field on the cathode and first 10 cm of propagation. The measured magnetic field profile is shown in Fig. 6 for half maximum charge on the B_z capacitor bank. Effectively, the field is zero at distances greater than 10 cm from the anode foil. A variety of cathode tips were used in the experiment as illustrated in Fig. 7, where the radial current density profiles shown are conceptual profiles for the case of large magnetic fields. For zero applied magnetic field, a Bennett profile beam rapidly evolves, independent of tip type. Examples of measured radial profiles for the bullet tip are shown in Fig. 8 for zero and finite magnetic fields. As illustrated schematically in Fig. 7, the bullet tip does produce a hollow beam with some current on axis.

The most important diagnostics in the experiment were the position monitors placed at various positions downstream. Net current and magnetic field centroid x and y data were recorded from three sets of loops.

Typical net current signals upstream and downstream are shown for zero and finite magnetic field values in Fig. 9. In general, finite magnetic field net currents are lower than zero field net currents, and the plasma current decay time is independent of magnetic field.

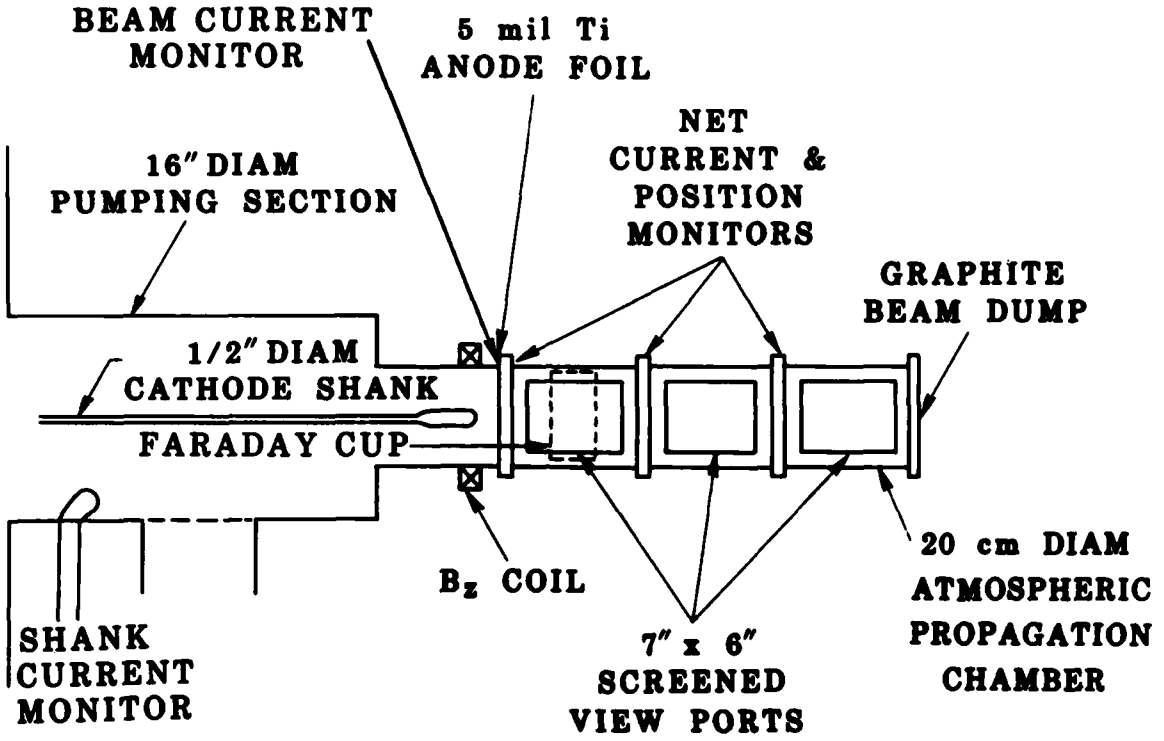

Figure 5. IBEX rotating hose experimental setup.

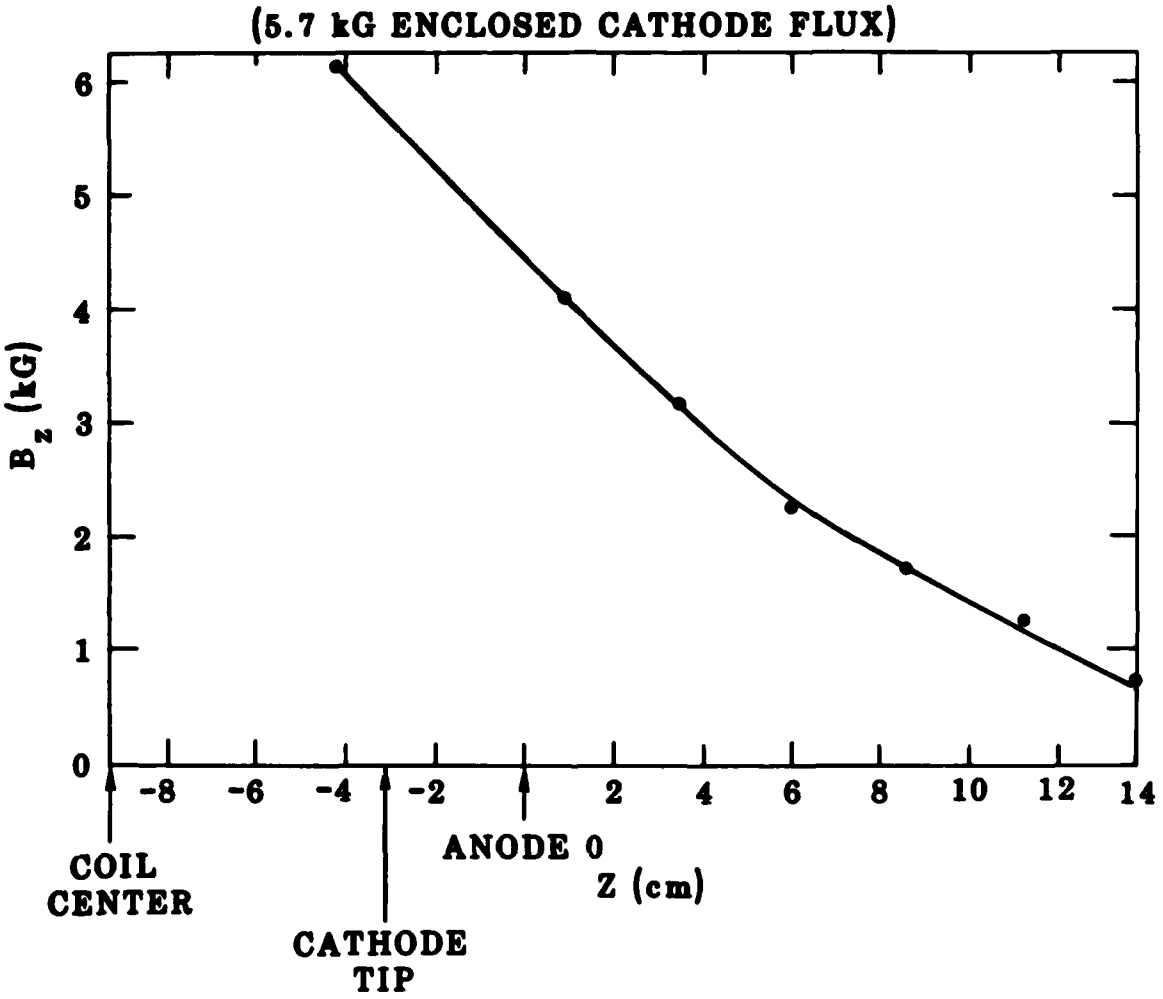

Figure 6. Measured magnetic field profile.

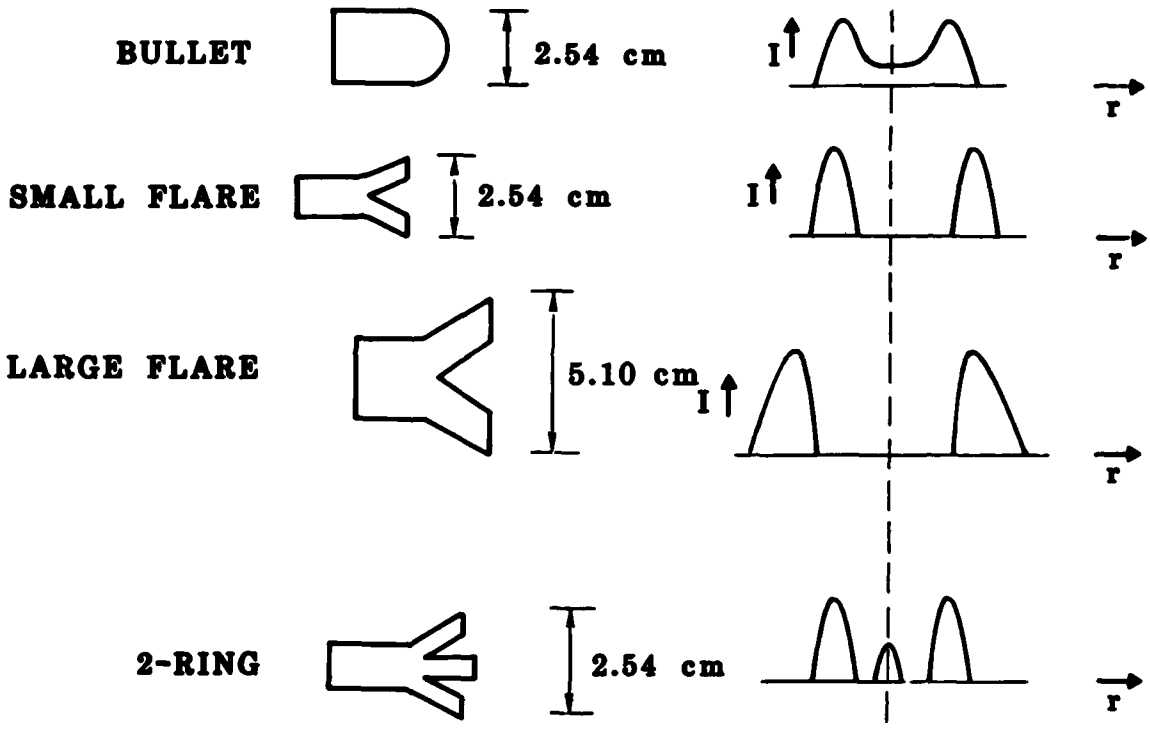

Figure 7. Cathode tips used and corresponding current densities.

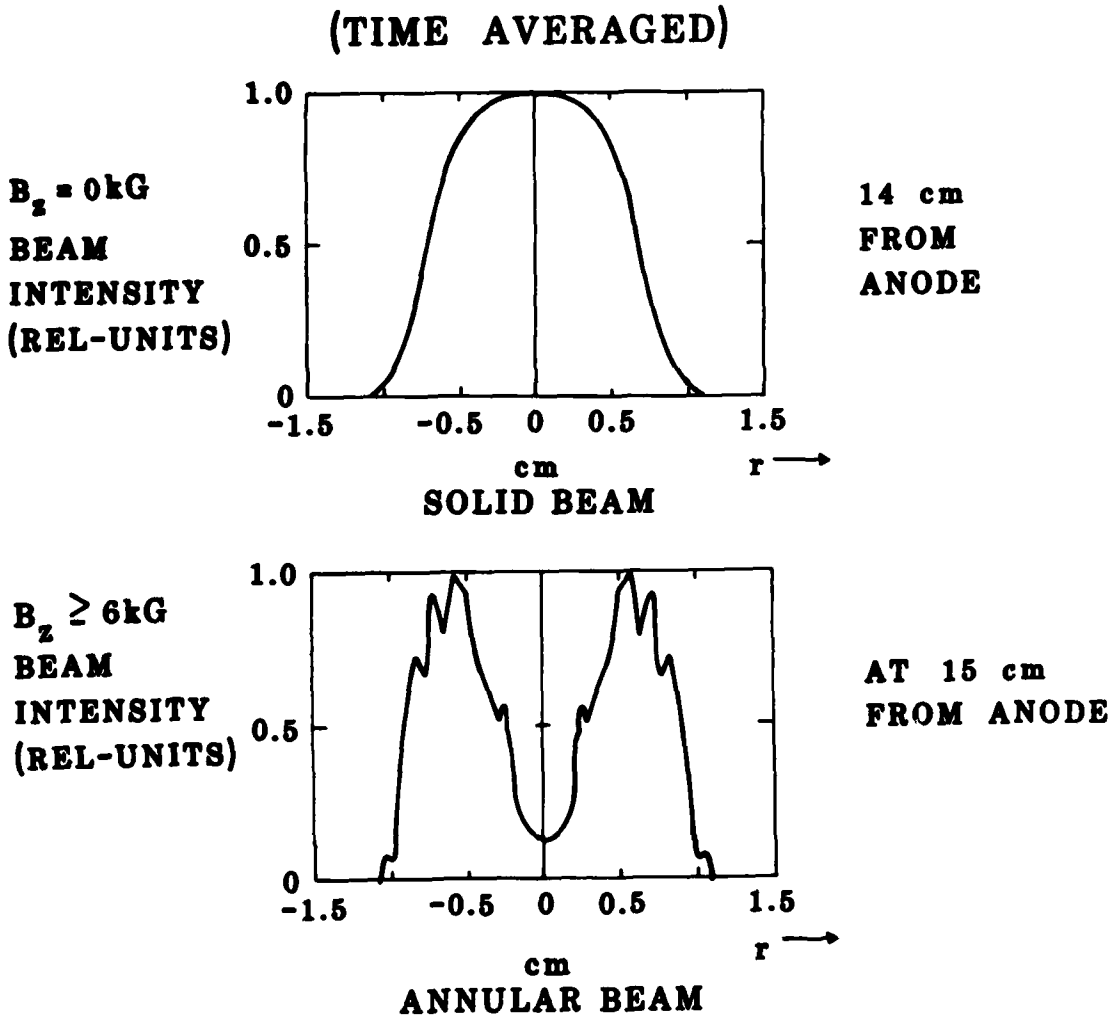

Figure 8. Foil bleaching corresponding to current density as a function of radius.

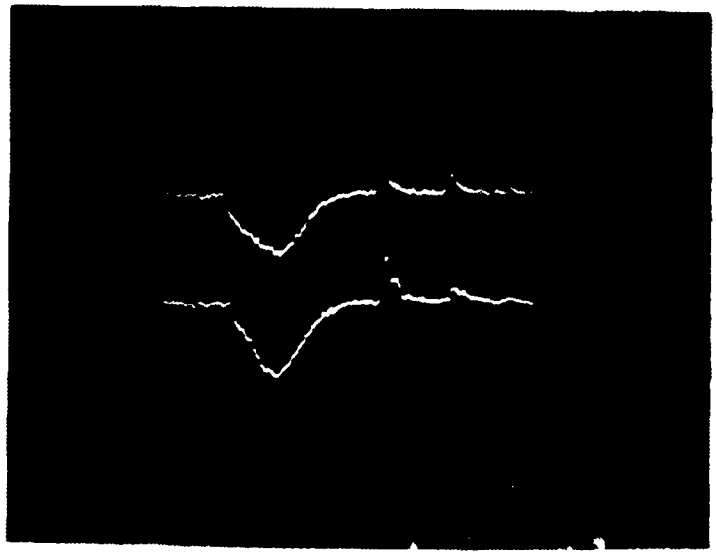

$B_z = 0$

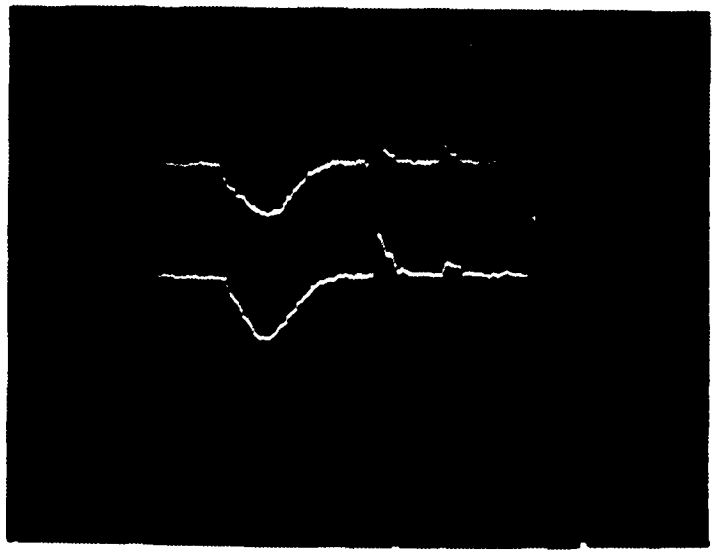

$B_z > 0$

Figure 9. Net current signals with and without a magnetic field.

The plasma decay time, τ_p, is effectively the inductive decay time of magnetic field energy in the drift tube, so it may be characterized by an inductance L and a plasma resistance R. As discussed below, the beam radius and area increase with magnetic field, so the inductance L decreases with magnetic field. The observation that τ_p is constant then implies that R decreases as the applied magnetic field increases. This is due to recombination, because as the beam area increases, the electron density decreases and the recombination rate decreases. The ionization rate, when summed over the total beam cross section is proportional only to current, so the total number of electrons per unit length then increases due to the decrease in recombination. Including this recombination effect, we find that $\tau_p \propto \sqrt{A}\, \ell n\ b/r$, or for our observed fixed τ_p, $A \propto 1/(\ell n\ b/r)^2$. This recombination effect is even more striking in the large cathode data, where the duration of the net current pulse is longer than in the data for the small cathodes.

The first task was to verify that a high quality beam was being produced in each case. We expect that the beam radius r should be given by

$$r^2 \simeq r_o^2 + \frac{r_c^4 \omega_c^2 I_A}{4c^2 I_{net}} \qquad (5)$$

where r_c is the cathode radius, $\omega_c = eB/\gamma mc$, $I_A = 4\pi\gamma mc/\mu_o e$ and I_{net} is the net current in the drift tube. This dependence was observed on blue cellophane data as shown in Fig. 10, where the observed radii are somewhat less than the radii predicted from Eq. (5). Note that r_o was determined by the measured radius at B = 0. This indicates that I_{net} is larger inside the beam than at the measurement point at the wall, which, in turn, suggests that a significant part of the plasma current is flowing outside the main beam channel. Based on these observations, we estimate the fraction of the plasma current flowing outside the beam as ~ 30%.

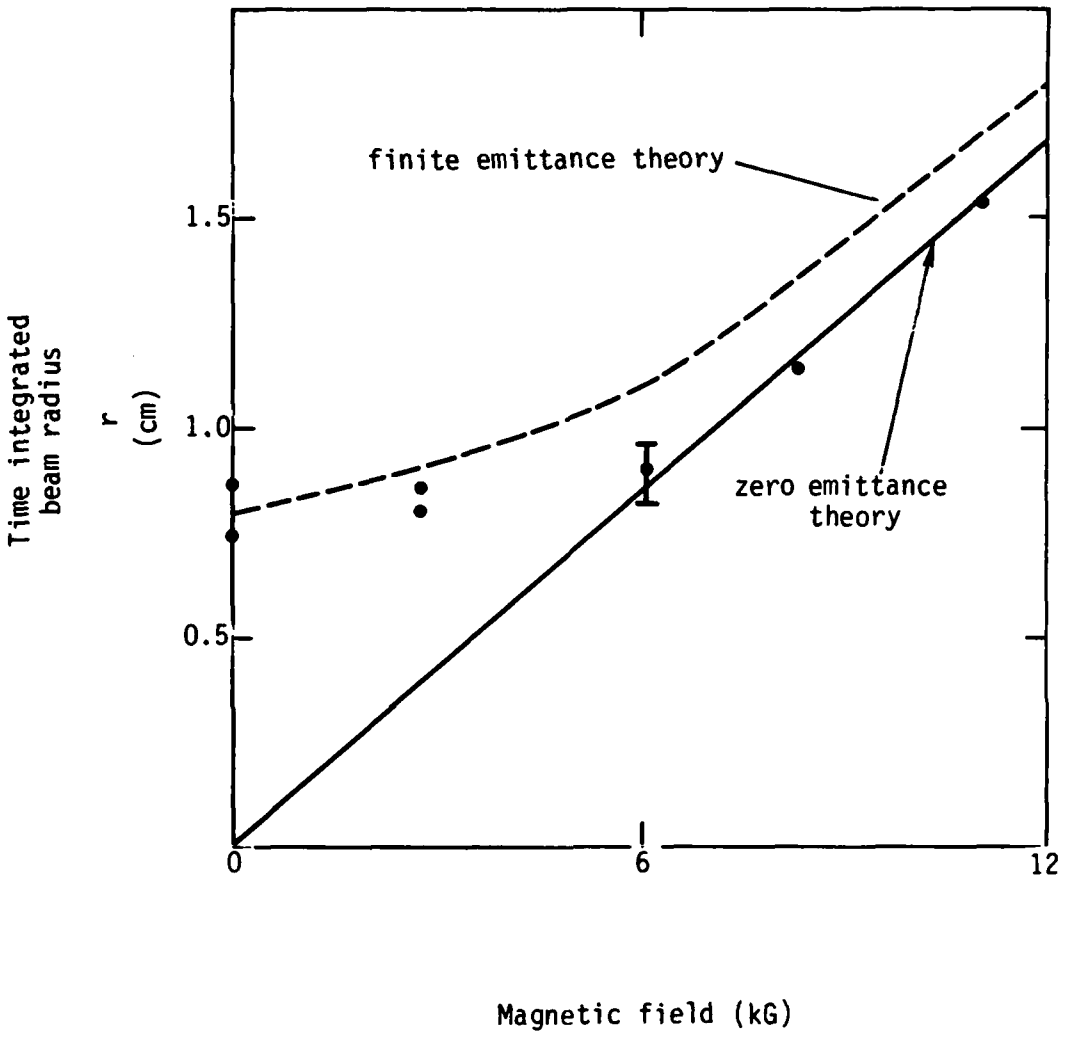

Figure 10. Equilibrium beam radius as a function of magnetic field.

We investigated the transition between the diode and gas region with a series of blue cellophane foils and with the Faraday cup array. Axial current density distributions inferred from this data are shown for a variety of positions in Fig. 11. For the case shown in Fig. 11, the beam is confined in the anode-cathode gap by the magnetic field so that particle orbits neither pinch nor diverge on average at the anode foil. In the absence of a pinch force, we would expect the particles to diverge along field lines to a radius of ~ 1.6 cm at 5 cm, as is observed. The reduction in applied magnetic field as a function of axial position causes the pinch force to begin to dominate beam dynamics at ~ 5 cm ($B_\theta > 2\ B_z$), and the beam begins to pinch. This pinch effect increases the beam emittance as demonstrated by the thickening of the beam annulus observed between 5 and 10 cm. Beyond 10 cm, the outer annulus is in equilibrium, as demonstrated by the similarity of profiles at 10 and 15 cm.

In the absence of a strong magnetic field, the beam comes into equilibrium within 5 cm of the anode foil. For the 'bullet tip' case, this implies radial velocities of greater than 0.1 c, derived simply by considering the observed radius reduction (1.27 cm to 0.8 cm over 5 cm) at injection. This beam pinch is certainly the dominant contribution to beam emittance, and it is exaggerated in the case of the large tip where the zero field radius is larger than for the other cathode tips.

The Faraday cup data confirms the blue cellophane data in the sense that peak Faraday cup signals occur where maximum bleaching is observed on the blue cellophane foils. In Fig. 12, Faraday cup signals from a typical bullet tip shot measured at 15 cm are shown. In this shot, the beam is slightly off center and r = +1 cm corresponds to the intense portion of the annulus. A rough empirical fit to much of the data shows that the current density falls off at large radii as $e^{-r/0.8\ cm}$ for $r \geq 2$ cm. This implies that less than 10% of the beam current is carried outside a 2 cm radius.

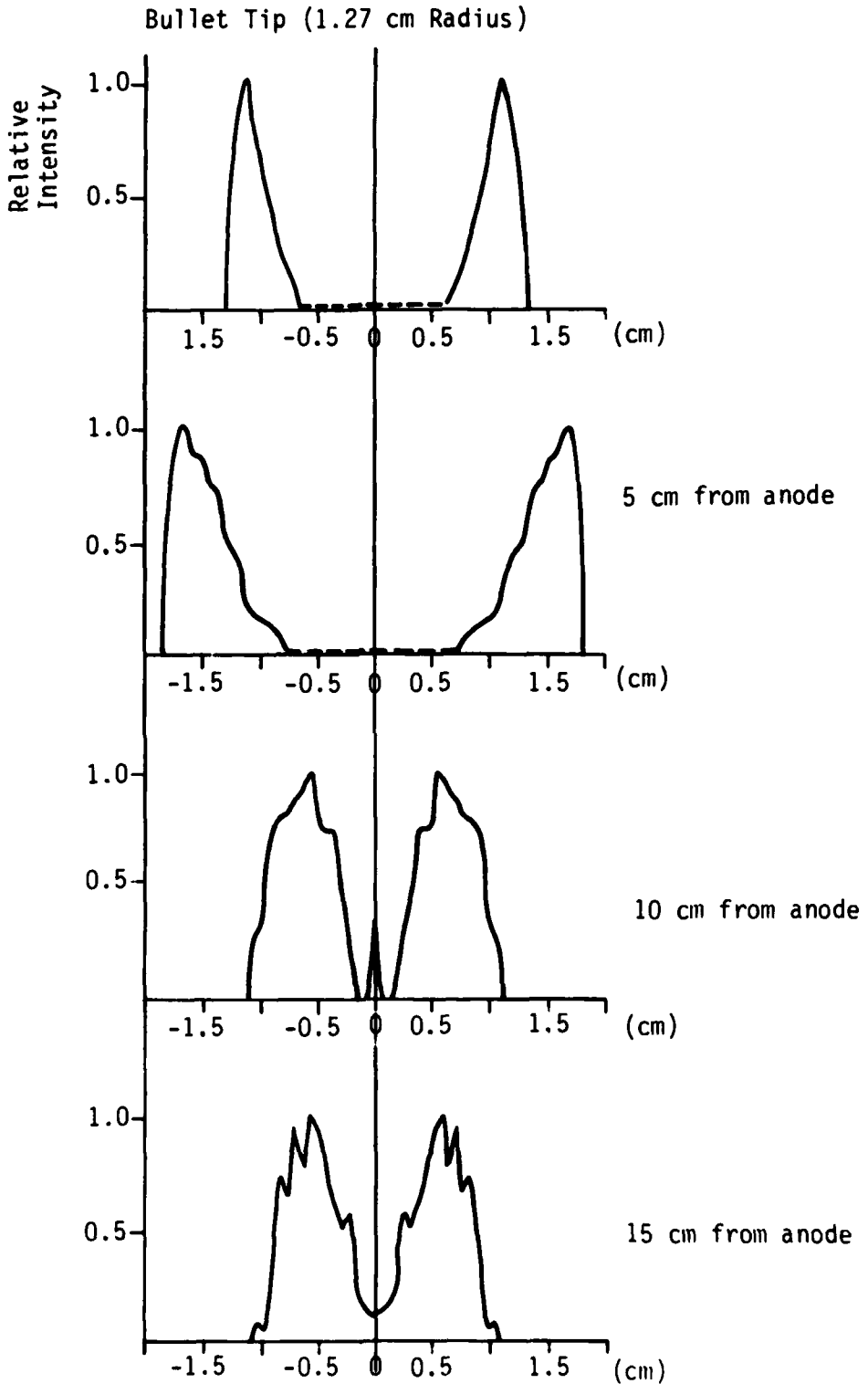

Figure 11. Radial profiles as a function of axial position.

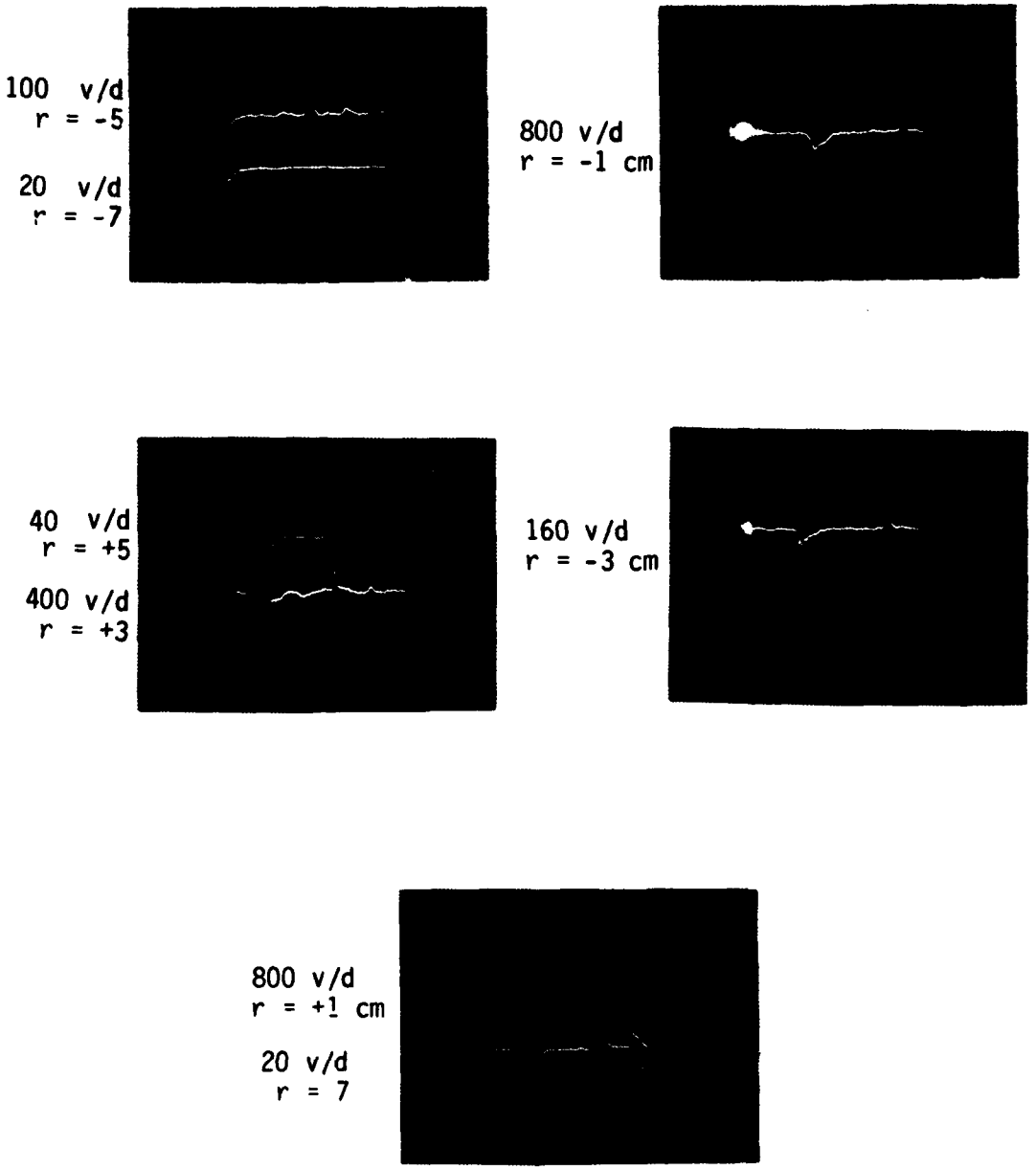

Figure 12. Faraday cup signals for a beam produced by a magnetized bullet tip.

Typical current density data at r = 0.9 cm for a zero field shot is shown in Fig. 13. In general, the zero magnetic field current density tends to be ~ 2-3 nanoseconds shorter than the current density for finite magnetic fields. We attribute this difference to the dynamics in the first few centimeters past injection. The abrupt change in equilibrium fields in the absence of an axial magnetic field results in high radial velocities throughout the pulse. We suggest that early and late in the pulse the beam does not pinch at all in the absence of a magnetic field.

Based on the symmetry observed in the equilibrium profiles, we conclude that a high quality beam is extracted, and that its radial profile is in good agreement with simple equilibrium theory. This theory also suggests that the effective net current is significantly (~ 1.3 times) higher than the wall net current due to currents flowing outside the beam. Plasma resistance is observed to decrease due to the increased area of magnetized beams.

Finally, we note that the magnetic field appears to facilitate pinched beam propagation early and/or late in the pulse.

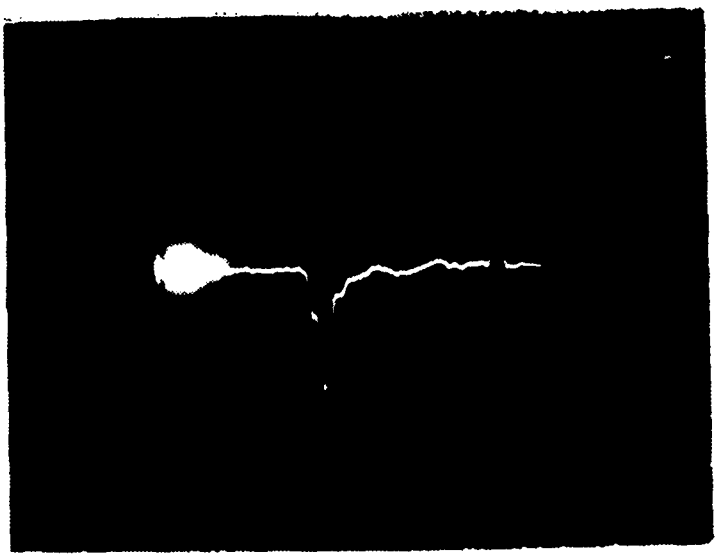

Figure 13. Zero field current density at r = .9 cm.

SECTION 3

HOSE GROWTH RESULTS

The primary goals of the experiment were to assess the effect of rotation on the hose instability and to find techniques involving rotation which might result in reduced hose instability growth.

Rotation gives us a technique for changing the radial beam distribution function in an arbitrary way. As shown in the previous section, we can make radical changes in the radial profile from shot-to-shot simply by applying a magnetic field. Without an applied field, the beam virtually always tends towards Bennett-type profiles. There is no reason to expect that Bennett profile beams will be most stable to the hose, so that in general, we may expect to find some other distribution function better than a Bennett.

The analysis of the data benefits from an understanding of where we expect to observe the instability in frequency space. In general, all linear theories predict that the frequency of the fastest growing mode is related to the dipole decay time by

$$\omega\tau_D \approx 0.4$$

where τ_D is the dipole decay time and ω is the hose angular frequency. In previous experimental work, we found that $\omega\tau_D \sim 0.1 - 0.4$. Noting that the typical value of τ_D ranges from 1 to 4 ns depending on conductivity, we expect hose frequencies in the range 8 - 20 MHz. The half periods associated with these frequencies are 16 - 64 ns. Since these times are comparable to the current waveform, which determines the slowest possible perturbation, we may conclude that the dominant hose frequency will appear to be that associated with the pulse length. In other words, the conductivity is sufficiently high that less than one hose oscillation will occur per pulse.

The discussion above is consistent with our observations and justifies interpretation of the maximum hose growth in terms of the maximum offset amplitude. Typical position monitor signals are shown in Fig. 14, which illustrate the low frequency nature of the instability.

There are two figures of merit for hose stabilization, the spatial growth rate k in cm^{-1}, and the growth rate normalized to the betatron wavelength λ_β. From our beam radius measurements we find that the betatron wavelength depends on the magnetic field as shown in Fig. 15 for the bullet and flared tip types.

The wavenumber k_h and normalized wavenumber $k_h\lambda_\beta$ are shown as a function of magnetic field for the high and low conductivity cases in Figs. 16-19. Values of the hose instability wavenumber are found by the formula

$$k_h = \frac{\ell n \left[\frac{x^2\ (37\ cm) + y^2\ (37\ cm)}{x^2\ (13\ cm) + y^2\ (13\ cm)}\right]^{1/2}}{24\ cm} \qquad (6)$$

and the error bars shown are standard errors averaged over the available data. It is clear from Figs. 16 and 17 that rotation dramatically reduces the hose growth rate k_h for both conductivity values. The normalized growth rate $k_h\lambda_\beta$ is also reduced by a factor of ~ 2.5 by the introduction of rotation.

This is a major result because by simply turning a knob, the propagation length is increased by a factor of 2-1/2. The effect is clear on open shutter photography, as shown in Fig. 20. The beam is clearly stabilized by rotation and the stable propagation distance is increased.

In several shots, propagation without measurable hose growth was observed, as shown in Figs. 21 and 22. In the case shown, the upper bound on growth is less than 2 - 3 times (less than one e-fold) over 85 cm - 6

a)

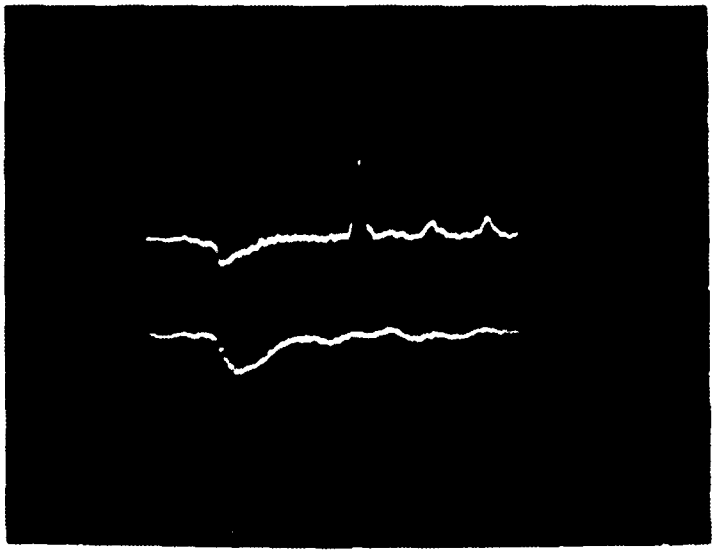

BEAM POSITION

b)

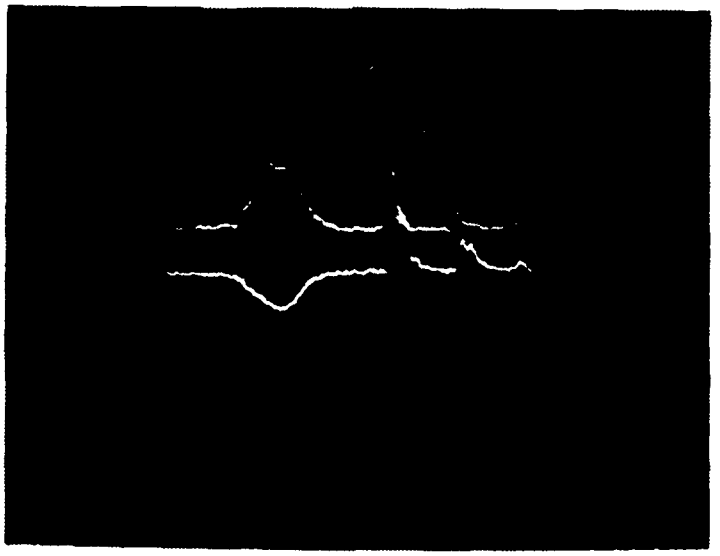

NET CURRENT

Figure 14. Typical position monitor signals.

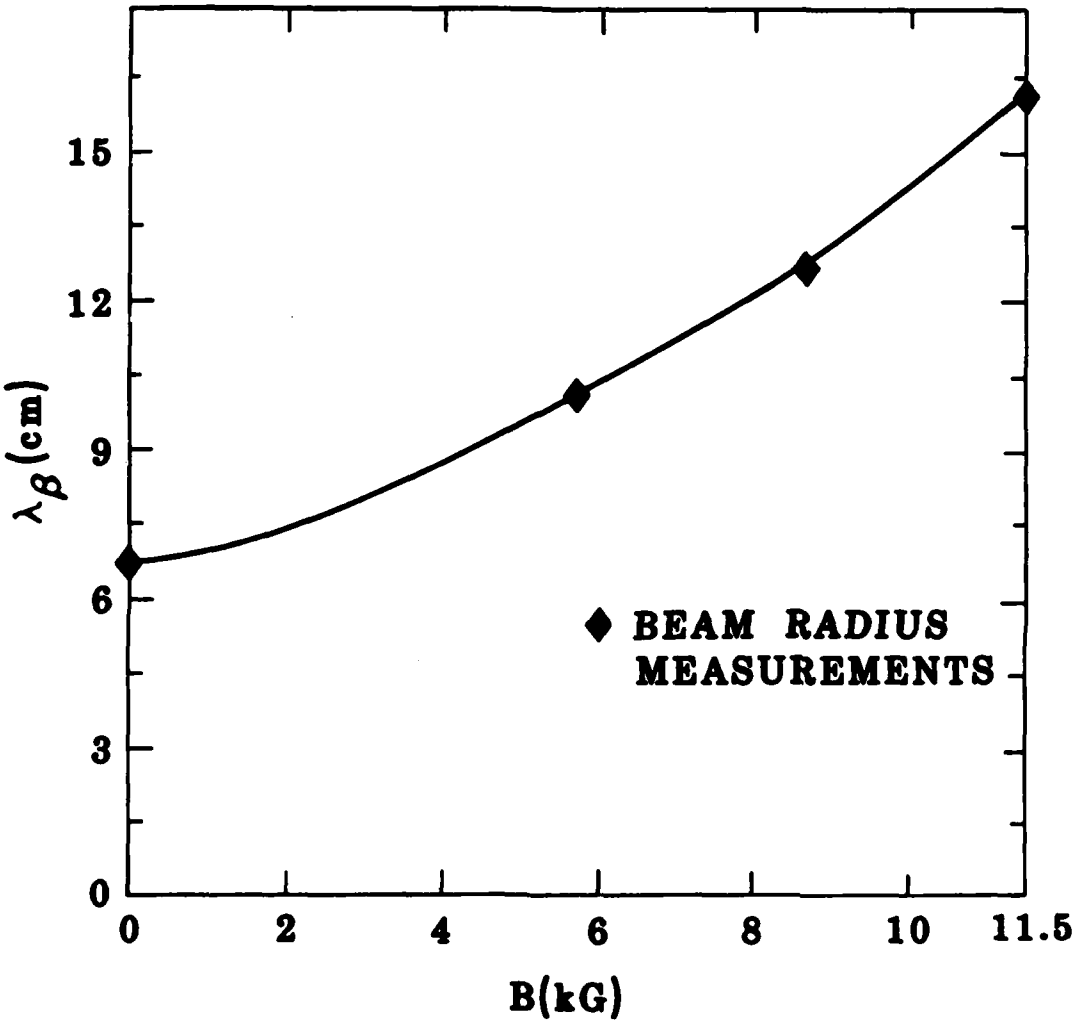

Figure 15. Betatron wavelength as a function of magnetic field.

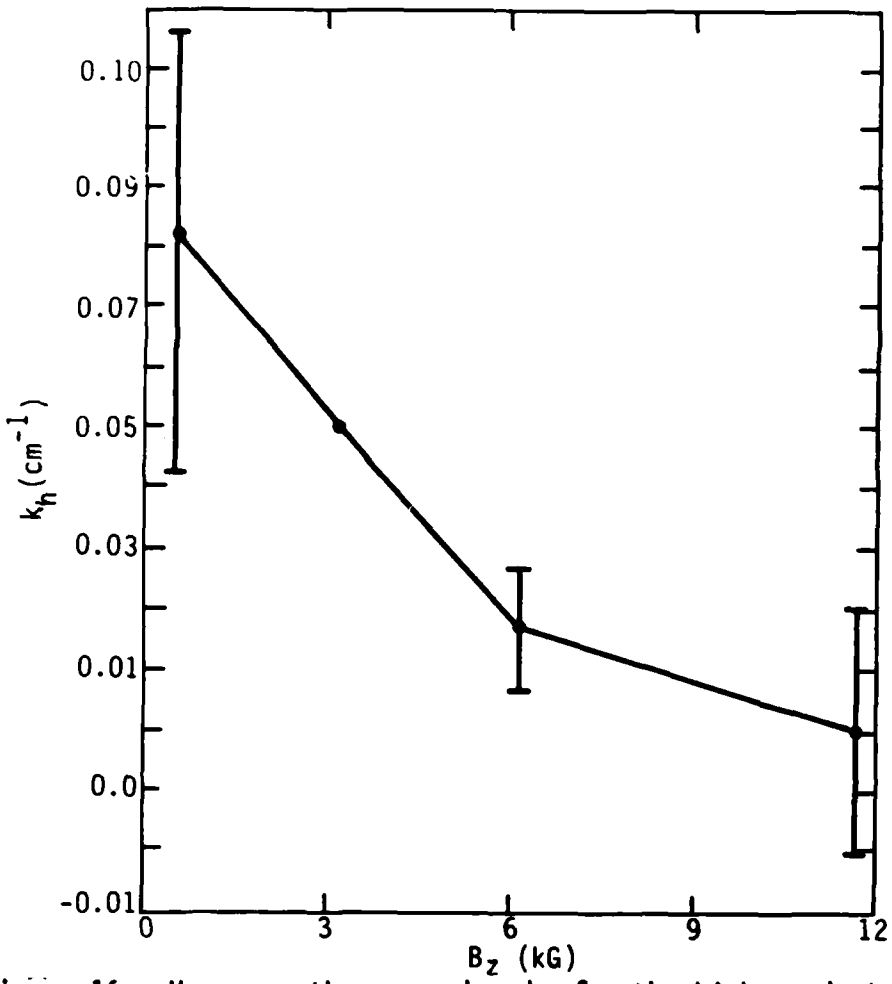

Figure 16. Hose growth wavenumber k_h for the high conductvity case.

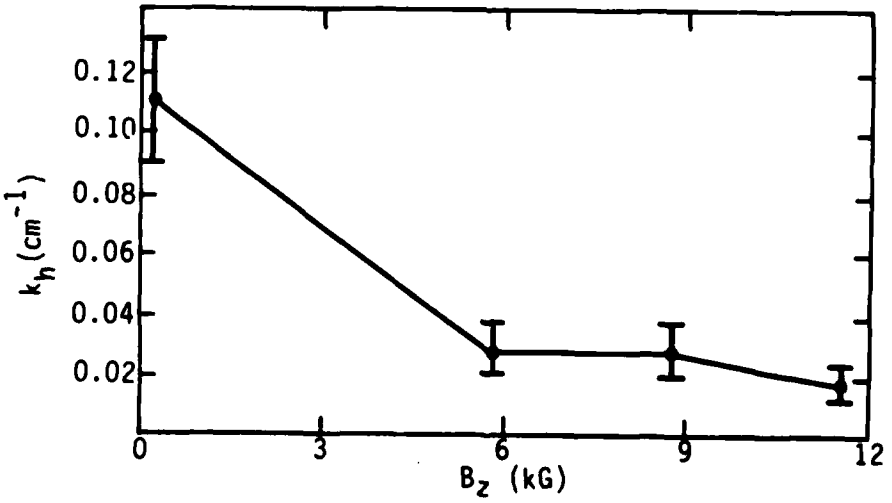

Figure 17. Hose growth wavenumber k_h for the low conductivity case.

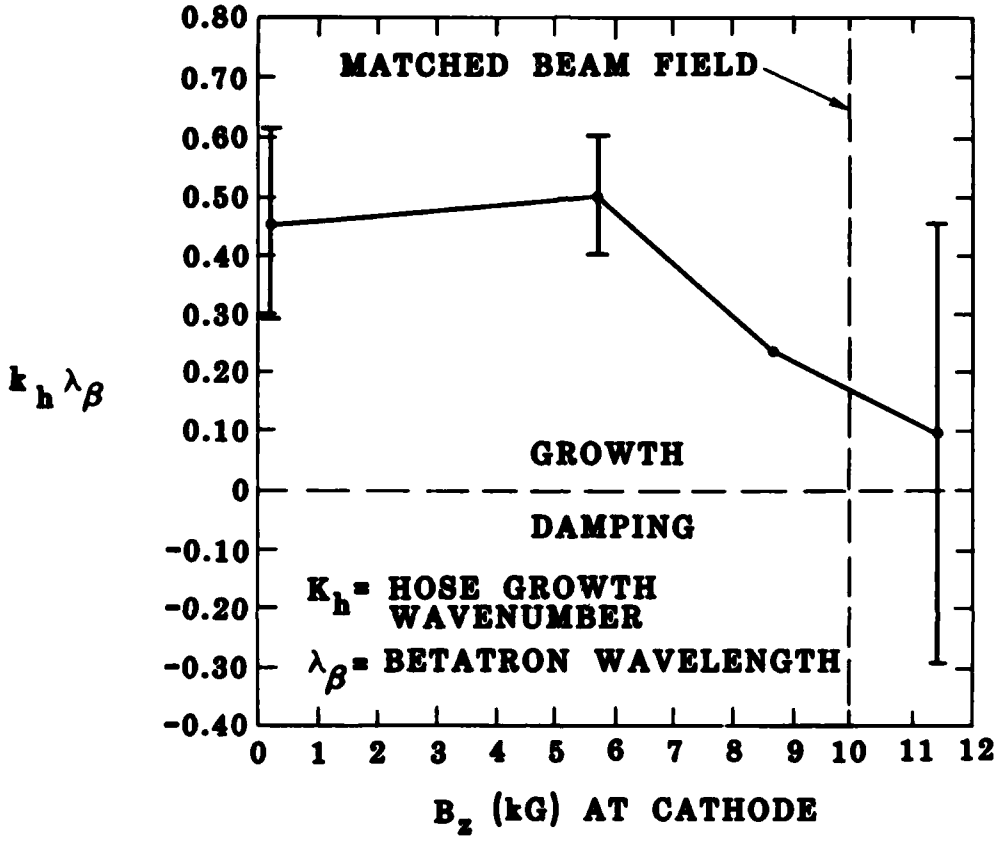

Figure 18. Normalized hose growth wavenumber $k_h \lambda_\beta$ for the high conductivity case.

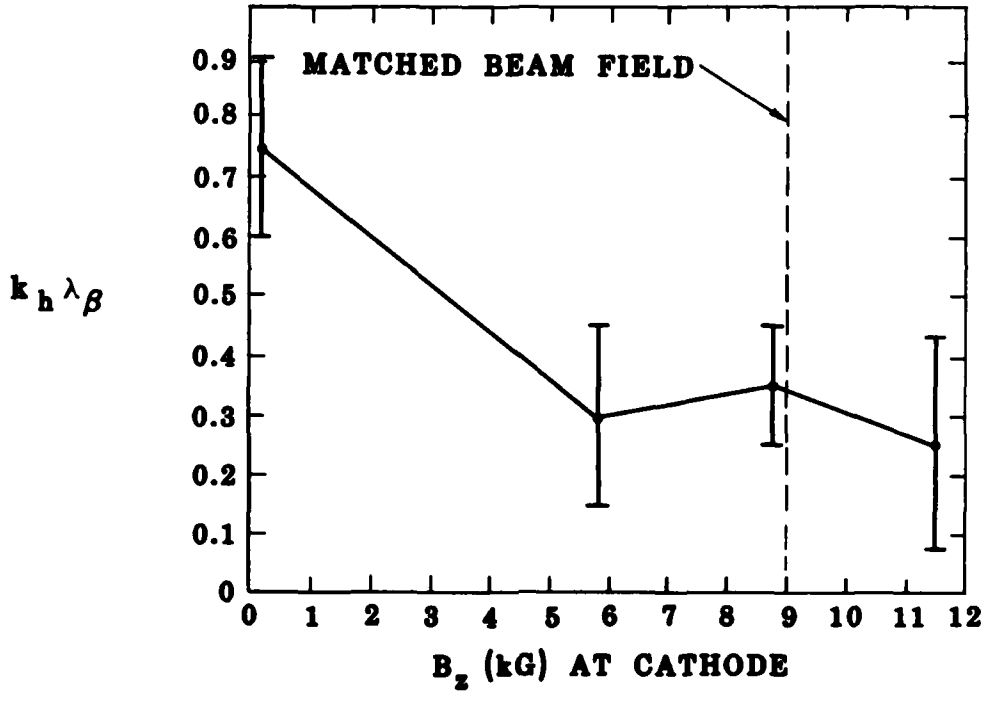

Figure 19. Normalized hose growth wavenumber $k_h \lambda_\beta$ for the low conductivity case.

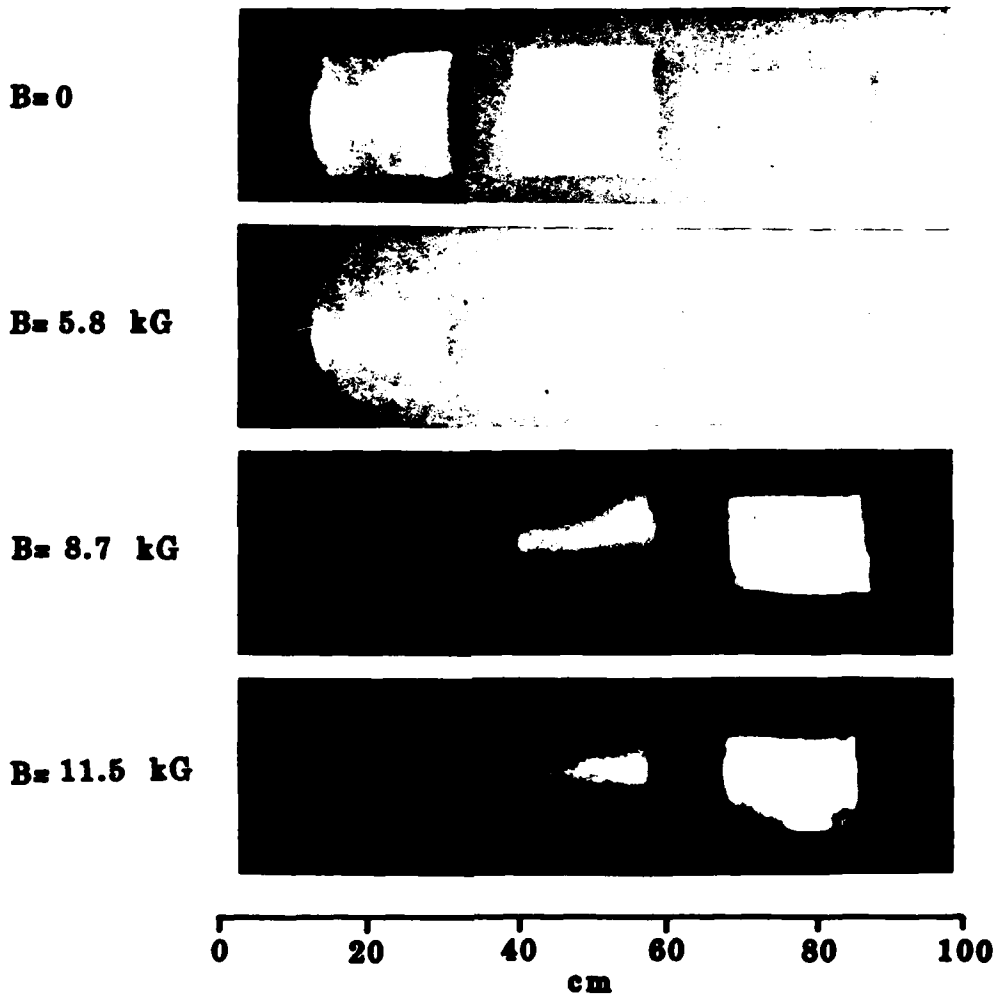

Figure 20. Open shutter photographs of the beam for various applied field values.

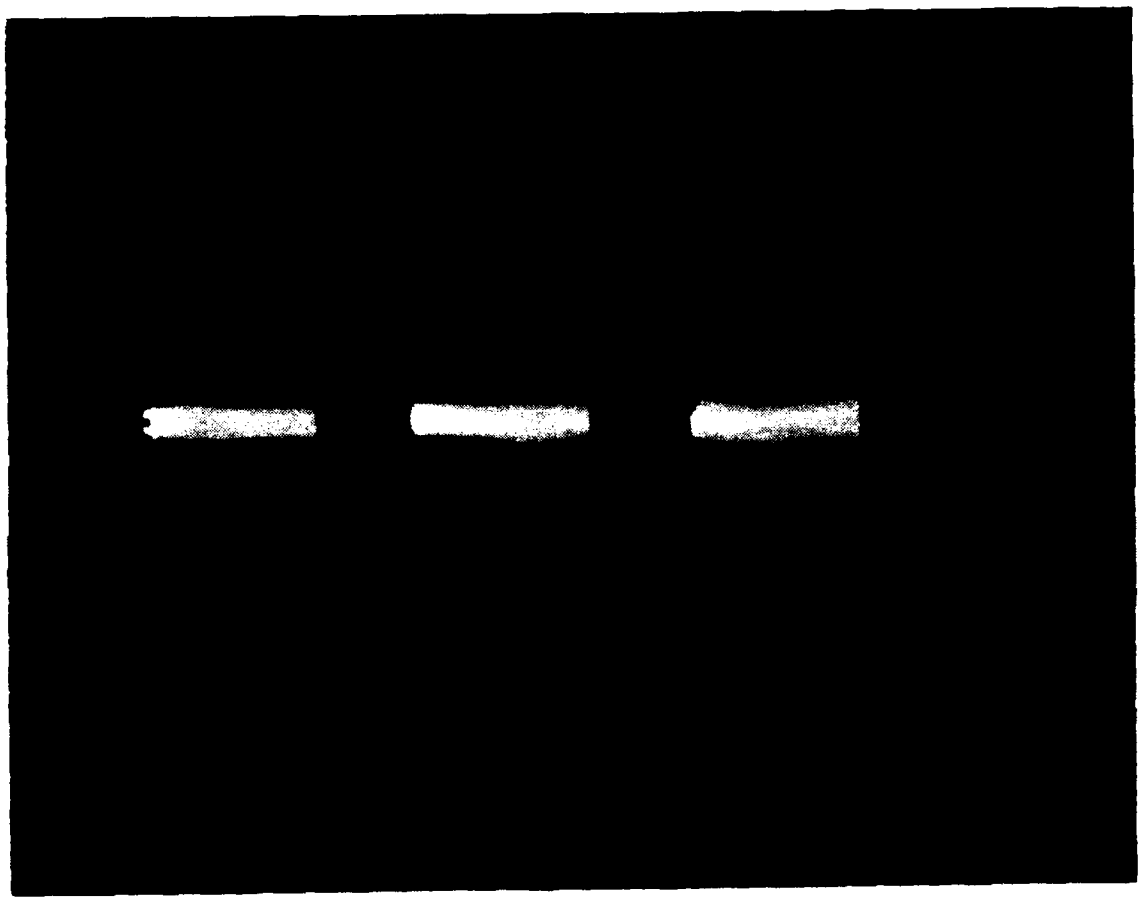

Figure 21. Open shutter photographs of hose stable beam propagation.

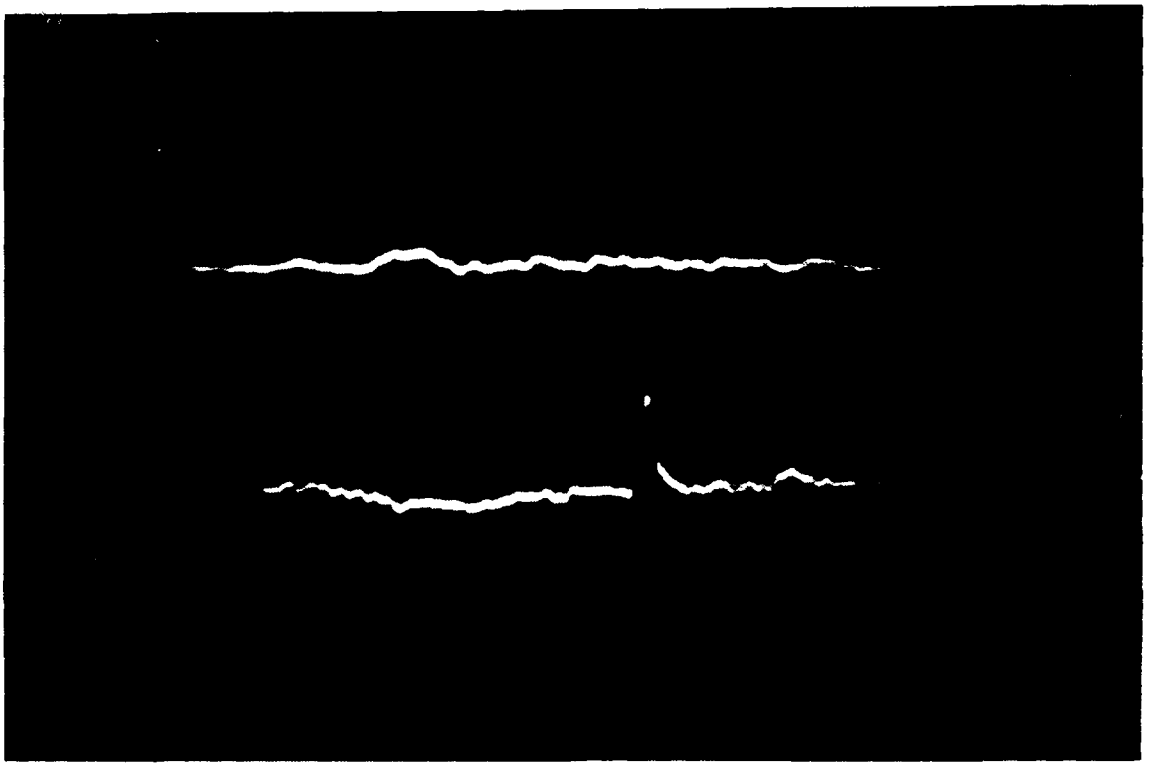

Figure 22. Position monitor traces for a stable beam.

betatron wavelengths. The best results were obtained when care was taken in aligning the axial magnetic field axis with the geometric axis defined by the drift tube.

The hose growth results obtained also vary with the type of cathode tip used. Best results were obtained with the 'bullet' tip cathode, while the annular cathode showed little, if any rotational hose suppression. The reason for this appears to be associated with the current on the axis of the beam. A comparison of data for the annular and double tip shots indicates that the double tip shots were, in general, much more stable. In fact, double tip beams generally have the same stability properties, growth rates, etc., as bullet tip beams. The nature of the instability in the annular tip case is not clear. For most of the shots taken in the IBEX series, open shutter photography is in good agreement with the position monitor signals in terms of the direction and magnitude of the instability. This is not the case for annular tip shots - as an example, the open shutter photograph shown in Fig. 23 for an annular tip shot is suggestive of filamentation.

Current on the beam axis would have a strong stabilizing effect on the filamentation. Data for the double tip shows a hose stabilization trend similar to that observed in the bullet tip case. In the double tip case, best results were obtained for a beam in which the beam equilibrium radii and cathode radii were nominally 'matched.' Matching the two radii appears to be important as the highly rotational, poorly matched case of the large flare cathode showed the highest hose growth.

To summarize, propagation of rotating beams with current in the center has been demonstrated to be more stable to the hose instability than propagation of non-rotating Bennett-type beams. Reductions in growth rate normalized to the betatron wavelength of order 2.5 have been observed for rotating beams with some current on axis. This result will be discussed further in Section 5.

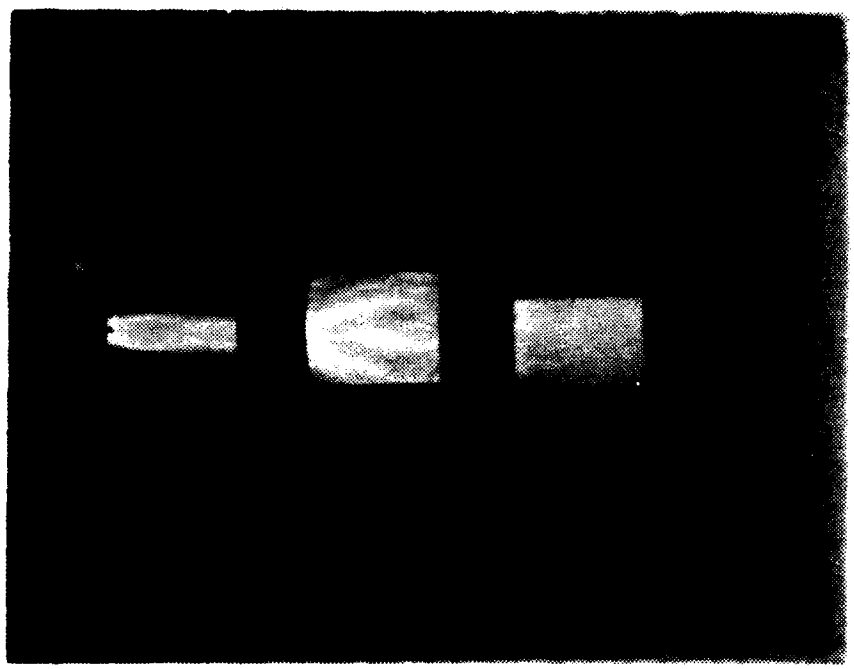

Figure 23. Annular, rotating beam propagation without current on axis.

SECTION 4

DISCUSSION

There are a number of physical effects which could result in stabilization of the resistive hose instability. It is worthwhile to briefly and succinctly restate the pertinent experimental data:

- The most stable cases are rotating annular beams with some small fractional current flowing on axis.

- Evidence exists for significant plasma current flow outside the beam cross section.

- The observed decay times (τ_D ~ 1-4 ns) are too long to allow more than one-half cycle of a hose oscillation to occur.

- Highly rotational beams are not stabilized.

- The rotation of beam return currents is larger than the rotation of the beam.

One obvious candidate for the stabilization mechanism is the added shear in betatron wavelength which results from rotation. This effect is increased in cases with some current on axis. For example, in the bullet cathode case, the central current betatron wavelength is ~30 cm where the outer current betatron wavelength was ~15 cm. Even in the absence of shear on axis, the shear in v_θ across the beam annulus is

$$\frac{\delta v_\theta}{v_o} \sim \frac{\delta_a}{a} .$$

As an example, for the typical case of $\delta a/a \sim 1/3$, we would have a differential rotation of π radians for a propagation distance of ~ 23 cm if $\lambda_\beta = 15$ cm. This rotational shear promotes phase mix damping even of low frequency perturbations.

A second rotational effect which may be of some importance is suggested by our diamagnetic loop measurements. In general, we find that total beam/plasma axial magnetic field is much less than expected based on the measured net current and rotation rate. This implies that the streamlines of plasma current have a much larger rotation or pitch than do the beam particles. A phase difference between beam and plasma current results, so that perturbations are not in phase. By contrast, with nonrotating beams, the beam and plasma perturbations are always in similar azimuthal phase.

Another difference between rotating and non-rotating beams is in the nature of the transverse temperature distributions. Beams produced at zero magnetic field are subjected primarily to radial forces such as the pinch force, so $v_r \gg v_\theta$. The rotation provides a mechanism by which we may expect, even for random components of the velocity, that

$$\langle v_r^2 \rangle < \langle (v - \bar{v}_\theta)^2 \rangle \qquad (7)$$

Thus, rotation implicitly changes the distribution in a fundamental way.

Increasing the dipole decay time by spreading the beam profile should have a stabilizing effect on the instability, because the beam centroid cannot go unstable more quickly than the magnetic fields diffuse. This is probably not a major stabilizing effect in our experiment, because the change in decay time due to profile changes is much less than the change in decay time due to other causes. The effect of decreasing τ_D by a factor of 3 through other causes is to increase growth by a factor of two, so we expect that smaller changes in τ_D due to profile changes will produce yet smaller changes in instability growth.

The observation that a significant current fraction (~ 30%) appears to flow outside the rotating beam could well be responsible for stabilization. The current fraction outside the beam in the absence of rotation was not measured so this hypothesis must remain speculative. Both broadened return current profiles and the increase in decay times are important high current mode issues, and our work suggests that both effects occurred in our experiment.

Finally, we note that Feinstein has suggested that the natural variation in radius with time introduced by the magnetized beam voltage and current rise-times in this experiment will stabilize the hose instability. We note that this effect also promotes channel broadening, which is also expected to reduce hose growth.

In general, the result of a broadened return current profile and a long decay time at high currents verify our present understanding of high current hose stabilization. This in itself is a very positive result.

SECTION 5
CONCLUSIONS

We have demonstrated a reduction in resistive hose instability growth rate of a factor of 2-3. This is accomplished by using annular, rotating, beam profiles with a small current in the center. Annular, rotating beams without current in the center were not found to be significantly more stable than conventional solid beam profiles.

We believe that these results have important implications for beam propagation experiments because they demonstrate a usable technique which leads to enhanced stability.

SECTION 6
ACKNOWLEDGEMENTS

The authors would like to thank Thomas Montoya and Ray Brown for expert technical assistance throughout the experiment. We would also like to thank Brendan Godfrey, Thomas Hughes, and Lawrence Wright for useful discussions. Finally, we would like to thank the many Rocketdyne, AFWL, and Sandia personnel who assisted us during our IBEX run.

REFERENCES

1. B. D. Guenther, R. Lontz, and J. L. May, "Particle Beams Research Issues," Proc. of the Part. Beam Res. Wkshp., US Air Force Academy, 9-11, January 1980.

2. E. P. Lee, Phys. Fluids, 21, 1327 (1978).

3. E. J. Lauer, R. J. Briggs, T. J. Fessenden, R. E. Hester and E. P. Lee, Phys. Fluids 16, 436 (1973).

4. K. G. Moses, R. W. Bauer and S. D. Winter, Phys. Fluids 16, (1973).

5. R. J. Adler, et. al., "Final Report - Beam Propagation Experimental Study," Mission Research Corporation, Albuquerque, AMRC-R-466, April 1983.

6. R. J. Adler, T. P. Hughes, G. F. Kiuttu, and B. Sabol, "Extraction and Propagation of an Intense Rotating Electron Beam," Mission Research Corporation, AMRC-R-422, Albuquerque, October 1982.

7. Rotating beam hose stabilization was first observed in the work of reference 6, and subsequently by M. G. Mazarakis in the so-called IBEX extraction experiments.

8. R. J. Adler, et. al., Rev. Sci. Instrum. 54, 9401 (1983).

END

FILMED

12-84

DTIC